Aalto University

Brange, F.; Samuelsson, P.; Karimi, B.; Pekola, J. P.

Nanoscale quantum calorimetry with electronic temperature fluctuations

Nanoscale quantum calorimetry with electronic temperature fluctuations

F. Brange and P. Samuelsson

Department of Physics and NanoLund, Lund University, Box 188, SE-221 00 Lund, Sweden

B. Karimi and J. P. Pekola

QTF Centre of Excellence, Department of Applied Physics, Aalto University, FI-000 76 Aalto, Finland

Motivated by the recent development of fast and ultrasensitive thermometry in nanoscale systems, we investigate quantum calorimetric detection of individual heat pulses in the sub-meV energy range. We propose a hybrid superconducting injector-calorimeter setup, with the energy of injected pulses carried by tunneling electrons. It is shown that the superconductor constitutes a versatile injector, with tunable tunnel rates and energies. Treating all heat transfer events microscopically, we analyze the statistics of the calorimeter temperature fluctuations and derive conditions for an accurate measurement of the heat pulse energies. Our results pave the way for fundamental quantum thermodynamics experiments, including calorimetric detection of single microwave photons.

I. INTRODUCTION

In quantum calorimetry [1], energy of individual particles is converted into measurable temperature changes. Mainly driven by the possibility of achieving unprecedented, high resolution and near-ideal efficiency x-ray detectors for space applications [1–4], quantum calorimetry has over the past few decades also been developed for a wide range of other particles, including α and β particles, heavy ions, and weakly interacting elementary particles [5–7]. Today, fast and sensitive thermometry, together with small absorbers with weak thermal couplings to the surrounding, allows for time-resolved measurements [8–11] and detection of energies all the way down to the far-infrared spectrum [12,13], i.e., energies of the order of meV.

Recent demonstrations of fast and ultrasensitive hot-electron thermometry [10,11] at cryogenic conditions constitute a key step towards quantum calorimetry for even smaller energies, around 100 μeV or less. Time-resolved detection of such low-energy quanta, carried, e.g., by microwave photons or tunneling electrons, is of fundamental interest for nanoscale and quantum thermodynamics. This includes heat and work generation in open systems [14–18], thermodynamic fluctuation relations [19–24], thermal quantum conductance [25], heat engines and information-to-work conversion [26,27], and coherence and entanglement [16]. However, calorimetric sub-meV measurements still constitute an outstanding challenge; a proof-of-principle experiment requires an improvement of the detection sensitivity by at least an order of magnitude and a source of heat pulses with well defined energy and controllable injection rate.

To meet this challenge we propose and theoretically analyze a nanoscale hot-electron quantum calorimeter coupled to a superconducting injector, see Fig. 1. As argued in Refs. [10,11], such setups show potential for superior detection sensitivity. All calorimeter heat transfer processes,

including the stochastic exchange of quanta with a weakly coupled thermal phonon bath, are treated on an equal, microscopic footing. This allows us to show that the rate and energy of the heat pulses injected from the superconductor, carried
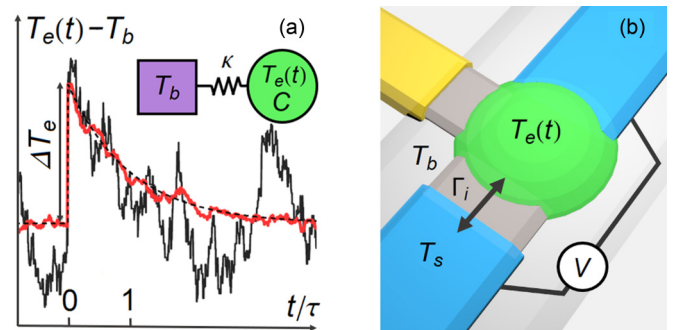

FIG. 1. (a) Two representative Monte Carlo simulated (see appendix) time traces of the absorber electron temperature $T_e(t)$, with a jump ΔT_e caused by a single particle absorption event followed by a decay, rate τ. The superimposed fluctuations are due to stochastic heat exchange with a phonon bath at low (red) and intermediate (black) temperatures T_b (see text). Noise free case, Eq. (1), is shown with a dashed line. Inset: Effective circuit model of a calorimeter with heat capacity C and heat conductance κ to the bath. (b) Schematic of the nanoscale injector-calorimeter setup: A normal metallic island (green) contains a thermalized electron gas, with fluctuating temperature $T_e(t)$, constituting the absorber. The island is well coupled to an electrically grounded superconductor (upper, blue) acting as a heat mirror. It is further tunnel coupled to another superconductor (lower, blue), kept at a temperature T_s and biased at a voltage V, serving as a particle source with tunable injection rate $\Gamma_i(T_s, V)$. A thermometer, coupled to the island, is also shown (yellow). The island phonons, at temperature T_b, constitute a thermal bath weakly coupled to the island electron gas.

by tunneling electrons, are tunable by the applied injector bias and temperature. Moreover, the varying pulse energy and stochastic injection give rise to temperature back-action effects modifying the calorimetric performance. Analyzing the resulting calorimeter temperature fluctuations, focusing on the experimentally accessible lowest order cumulants, we derive conditions for a faithful operation, where back-action effects are negligible. Our results will stimulate fundamental experiments, aiming for thermal measurements of, e.g., single microwave photons.

II. HOT-ELECTRON QUANTUM CALORIMETRY

A generic hot-electron quantum calorimeter is shown schematically in Fig. 1(a): An absorber with heat capacity C is coupled, with thermal conductance κ, to a heat bath of phonons kept at temperature T_b. The absorber electron gas is rapidly thermalizing, with a temperature $T_e(t)$ well defined at all times. Operating in the linear regime and neglecting temperature background noise, absorbing a particle with energy ε at $t = 0$ gives rise to a jump $\Delta T_e = \varepsilon/C$ of the absorber temperature, followed by an exponential-in-time decay as

$$T_e(t) = T_b + \Delta T_e e^{-t/\tau}, \quad t \geqslant 0 \tag{1}$$

with $\tau = C/\kappa$ the absorber relaxation time. With a noninvasive and fast temperature measurement, ΔT_e and thus the energy ε can be inferred. However, the background temperature exhibits fluctuations $\delta T_e(t)$, due to the fundamentally stochastic bath-absorber energy transfer, governed by the fluctuation-dissipation-like relation

$$\langle \delta T_e(t) \delta T_e(t') \rangle = \frac{k_B T_b^2}{C} e^{-|t-t'|/\tau}, \tag{2}$$

see Fig. 1(a) for two different temperatures. Hence, the background noise is typically negligible if the amplitude $\sqrt{\langle \delta T_e^2(t) \rangle} = T_b (k_B/C)^{1/2}$ is much smaller than the temperature signal ΔT_e; larger noise prevents a faithful absorber temperature readout.

The condition $\Delta T_e \gg \sqrt{\langle \delta T_e^2(t) \rangle}$ is met in state-of-the-art experiments [10] with real-time detection of $\varepsilon \sim 100$ meV, where the signal-to-noise ratio $\Delta T_e/\sqrt{\langle \delta T_e^2 \rangle} = \varepsilon/[T_b \sqrt{k_B C}] \sim 100$ (for $T_b \sim 100$ mK, $C \sim 10^5 k_B$). To accurately detect $\varepsilon \lesssim 100$ μeV requires significantly reduced C and T_b (details to be discussed in the section on experimental feasibility). While detection of heat pulses $\varepsilon \lesssim 100$ μeV is within reach, albeit challenging, a proof-of-principle experiment also requires an injector with controllable ε and tunable injection rate Γ_i, such that the heat pulses are well separated in time, $\tau \Gamma_i \ll 1$.

Here we propose and analyze an integrated hybrid superconductor injector calorimeter, see Fig. 1, fulfilling all requirements. The injected heat pulses are carried by tunneling quasiparticles. Both the injector-absorber (i) and bath-absorber (b) heat exchanges are described microscopically, with quanta of energy transferred at rates $\Gamma_\sigma(T_e)$, $\sigma = $ i, b. The statistics of the heat pulses is described by the cumulant generating functions (CGFs) $F_\sigma(\xi_\sigma, T_e)$ for the long-time,

total energy transfer [28],

$$F_\sigma(\xi_\sigma, T_e) = \Gamma_\sigma(T_e) \left[\int d\varepsilon \, e^{i\varepsilon\xi_\sigma} P_\sigma(\varepsilon, T_e) - 1 \right], \tag{3}$$

for uncorrelated, Poissonian particle transfers. Here ξ_i, ξ_b are counting fields and the particle energies are distributed according to $P_\sigma(\varepsilon, T_e)$, accounting for fluctuations of energy due to quantum and/or thermal effects, generic for nanosystems. We first investigate the CGFs at constant T_e and then analyze the back action of the temperature fluctuations on the energy transfer rates, deriving estimates on the system parameters required for a faithful calorimetric operation.

A. Hybrid nanoscale calorimeter

The injector-calorimeter system [see Fig. 1(b)] consists of a superconducting injector, with gap Δ and fixed temperature T_s, tunnel coupled, with a (normal state) conductance G_T, to a nanoscale metallic island absorber of volume $\mathcal{V}$. The absorber electron gas has a temperature $T_e(t)$ and heat capacity $C[T_e(t)] = (\pi^2 k_B^2/3)\nu_F T_e(t)$, with ν_F the density of states (DOS) at the Fermi level. The electron gas is further coupled [29], with a thermal conductance $\kappa[T_e(t)] = 5\Sigma \mathcal{V} T_e^4(t)$ with $\kappa \equiv \kappa(T_b)$ and Σ the electron-phonon coupling constant, to the bath phonons kept at a fixed temperature T_b. A second superconductor, coupled to the absorber via an Ohmic contact, works as a heat mirror and fixes the electric potential of the island to the superconducting chemical potential. A bias $|V| < \Delta/e$ is applied between the injector and the second superconductor. The temperature $T_e(t)$ is measured by a fast, ultrasensitive thermometer, assumed to be effectively noninvasive [30]. We neglect both standard and inverse proximity effect.

Injector-absorber heat pulses are transferred by the tunneling of individual electron and hole quasiparticles. The statistical properties of the charge transfer across a normal-superconducting tunnel barrier are well known [31,32]. By properly accounting for the energy carried by each tunneling particle [33], the generating function $F_i(\xi_i, T_e)$ for the heat transfer statistics is readily obtained as

$$F_i(\xi_i, T_e) = \int d\varepsilon [\Gamma_+^i (e^{i\xi_i\varepsilon} - 1) + \Gamma_-^i (e^{-i\xi_i\varepsilon} - 1)] \tag{4}$$

with rates $\Gamma_\pm^i(\varepsilon) = (G_T/e^2)\nu_S(\varepsilon - eV) f_\pm(\varepsilon - eV, T_s) f_\mp(\varepsilon, T_e)$ where $\nu_S(\varepsilon) = |\varepsilon|/\sqrt{\varepsilon^2 - \Delta^2}\theta(|\varepsilon| - \Delta)$, with $\theta(\varepsilon)$ the step function, is the normalized superconducting DOS and $f_+(\varepsilon, T) = (e^{\varepsilon/[k_B T]} + 1)^{-1}$, $f_-(\varepsilon, T) = 1 - f_+(\varepsilon, T)$. From the first and second derivatives of $F_i(\xi_i, T_e)$ with respect to ξ_i (taken at $\xi_i \to 0$), the known expressions for the average energy current and noise [34] are obtained. Equation (4) describes particles tunneling in (+) and out (−) of the absorber with spectral rates $\Gamma_\pm(\varepsilon)$. The energy of each particle is "counted" via the factors $e^{\pm i\xi\varepsilon}$. By comparing Eqs. (3) and (4) [changing $\varepsilon \to -\varepsilon$ in the second term in (4)] we see that the injector provides uncorrelated-in-time energy transfer events, at a rate $\Gamma_i(T_e) = \int d\varepsilon[\Gamma_+^i(\varepsilon) + \Gamma_-^i(\varepsilon)]$, with an energy probability distribution $P_i(\varepsilon, T_e) = [\Gamma_+^i(\varepsilon) + \Gamma_-^i(-\varepsilon)]/\Gamma_i$.

Focusing on the regime $k_B T_s, k_B T_e \ll \Delta$, the CGF $F_i(\xi_i, T_e)$ describes four superimposed Poissonian processes with injections at energies $\pm\Delta \pm eV$, see appendix. In
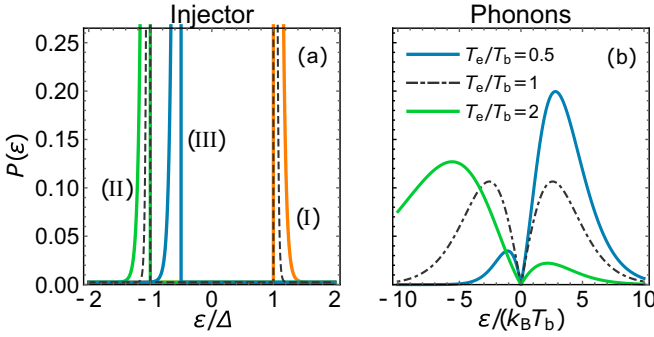
FIG. 2. (a) Probability distribution of energies transferred to the absorber $P(\varepsilon)$ from injector-absorber quasiparticle tunneling, for four different sets of $\{k_B T_s/\Delta, k_B T_e/\Delta, eV/\Delta\} = \{0.02, 0.02, 0\}$ (dashed), $\{0.05, 0.01, 0\}$ (orange, solid), $\{0.01, 0.05, 0\}$ (green, solid), and $\{0.01, 0.05, 0.5\}$ (blue, solid). Corresponding injector regimes (I), (II), and (III) shown, see text. (b) Probability distribution for bath-absorber energy transfers due to phonon creation and annihilation, for different temperature ratios T_e/T_b.

particular, in three different limits $V = 0$, $T_s \gg T_e$ (I), $V = 0$, $T_s \ll T_e$ (II), and $T_s(1 - e|V|/\Delta) \ll T_e \ll e|V|/k_B$ (III), particles are injected at corresponding energy $\varepsilon_I = \Delta$, $\varepsilon_{II} = -\Delta$, and $\varepsilon_{III} = eV - \Delta$, see Fig. 2(a), giving CGFs

$$F_i^{(\alpha)}(\xi_i, T_e) = g c_\alpha (e^{i\varepsilon_\alpha \xi_i} - 1), \quad \alpha = \text{I,II,III}, \quad (5)$$

where $g = \sqrt{2\pi} G_T \Delta/e^2$ and $c_I = h(T_s)$, $c_{II} = h(T_e)$ and $c_{III} = h(T_e) \exp([e|V|/k_B T_e]/2)$, with $h(T) = \sqrt{k_B T/\Delta} \exp(-\Delta/[k_B T])$.

Equation (5) is the first key technical result of this paper. It shows that, by tuning the externally controllable T_s and V, we can reach three different regimes where the tunnel-coupled superconductor injects particles with a well-defined energy ε_α, at a rate $g c_\alpha$. This demonstrates that the superconductor constitutes a versatile heat pulse injector, required for the proposed proof-of-principle quantum calorimeter experiment. Moreover, for small temperature deviations $T_e - T_b \ll T_b$, relevant for the calorimeter operation, we have

$$\Gamma_i = g[h(T_s) + h(T_b) \cosh(eV/k_B T_b)]. \quad (6)$$

Under the conditions $C = 10^3 k_B$, $T_b = 30$ mK, the relaxation time τ is approximately 1–10 μs [10,35]. Experimentally $g \sim 10^{10}$–10^{12} s^{-1} if the injector resistance G_T^{-1} varies in the range 3–300 kΩ [10,35], making the individual injection event condition $\Gamma_i \tau \ll 1$ accessible by tuning T_s, V. The injector is assumed to have ideal BCS (Bardeen-Cooper-Schrieffer) DOS. However, realistic tunnel junctions present nonzero leakage with zero-bias conductance γG_T attributable to subgap states, absent in the BCS DOS. This leads to an additional tunneling rate at subgap energies, $\Gamma_i^0 = \gamma g T_e/\Delta$, which however for standard $\gamma \sim 10^{-5}$ is negligible compared to Γ_i.

Microscopically, the bath-absorber energy transfer is due to creation and annihilation of individual bath phonons. Assuming a weak coupling between the phonons and the absorber electrons, the CGF $F_b(\xi, T_e)$ of the energy transfer is written in the form of Eq. (4), with the spectral rates given by the text book result [36] for phonons in a metal, $\Gamma_\pm^b(\varepsilon) = -\Sigma \mathcal{V}/[24 k_B^5 \zeta(5)]\varepsilon^3 n(\pm\varepsilon, T_b) n(\mp\varepsilon, T_e)$,

where $n(\varepsilon, T) = (e^{\varepsilon/[k_B T]} - 1)^{-1}$ and $\zeta(x)$ the Riemann zeta function. Similar to the injector, from $\Gamma_\pm^b(\varepsilon)$ one gets $\Gamma_b(T_e) = \int d\varepsilon[\Gamma_+^b(\varepsilon) + \Gamma_-^b(\varepsilon)]$ and $P_b(\varepsilon, T_e) = [\Gamma_+^b(\varepsilon) + \Gamma_-^b(-\varepsilon)]/\Gamma_b$, with the energy probability distribution plotted in Fig. 2(b) for a set of temperature ratios T_e/T_b. It is clear from the figure that, in contrast to the sharply peaked and gapped injector-absorber energy distribution, the bath-absorber distribution is broad and smooth, symmetric around $\varepsilon = 0$ for $T_e = T_b$.

The cumulants $S_b^{(n)} = \partial_{\xi_b}^n F_b(\xi_b, T_e)|_{\xi_b=0}$ are given by

$$S_b^{(n)} = \Sigma \mathcal{V} k_B^{n-1} \frac{\zeta(n_\pm)(n+3)!}{24\zeta(5)}(T_e^{n+4} \pm T_b^{n+4}), \quad (7)$$

where $n_\pm = n + (7 \pm 1)/2$ and $+/-$ is for $n = 1, 2...$ even/odd. The result for odd n is exact and for even n an accurate approximation, deviating $<2\%$ from the exact result for any n, T_e/T_b [37,38], see appendix. Equation (7) is our second key technical result, which gives a complete description of the statistics of the electron-phonon heat transfer. Besides being a fundamentally interesting result on its own, it is a prerequisite for the analysis of the temperature fluctuation statistics below. We note the well-known result $S_b^{(1)} = \Sigma \mathcal{V}(T_e^5 - T_b^5)$ [29,38].

III. TEMPERATURE FLUCTUATION STATISTICS

While the average temperature in hybrid nanoscale systems has been widely investigated [39], there is to date no experimental investigation of the temperature noise. To obtain a complete picture of the fluctuations, we investigate the full temperature statistics [40–43], however, focusing on the noise.

Both rates $\Gamma_\sigma(T_e)$ and probabilities $P_\sigma(\varepsilon, T_e)$ generally depend on $T_e(t)$. For a large rate Γ_i, the time average $\overline{T}_e$ might deviate notably from T_b. Moreover, as a result of the stochastic energy transfers, $T_e(t)$ develops slow fluctuations in time, on the scale of τ. Both these effects act back on the transfer statistics and might alter the calorimetric operation. Fully accounting for this back action, we analyze the distribution $P(\theta)$ of the low-frequency, time integrated absorber temperature fluctuations $\theta = \int[T_e(t) - \overline{T}_e]dt$. $P(\theta)$ and the cumulants are obtained within a stochastic path integral approach [44], following [28]. This allows us to derive conditions for optimal calorimeter performance.

The distribution is plotted in Fig. 3(a) for the regimes (I) and (II), with injection at energies $\pm\Delta$, at $\tau\Gamma_i \ll 1$. As a consequence of the heat pulses being well separated in time, the deviations from the average $T_b t_0$ are small (t_0 is the measurement time). However, the two distributions are clearly non-Gaussian, shifted and skewed in opposite temperature directions. Both the average electron temperature $\overline{T}_e$ and the cumulants $S_{T_e}^{(n)}$ can be expressed in terms of $\langle\langle \mathcal{E}^n(T_e) \rangle\rangle = (-i)^n \partial_\xi^n F(\xi, T_e)|_{\xi=0}$, the cumulants of the absorber energy currents. Here $F(\xi, T_e) = F_i(\xi, T_e) + F_b(\xi, T_e)$. The average temperature $\overline{T}_e$ is found from the energy conservation condition $\langle \mathcal{E}(\overline{T}_e) \rangle = 0$. The second and third cumulants are given
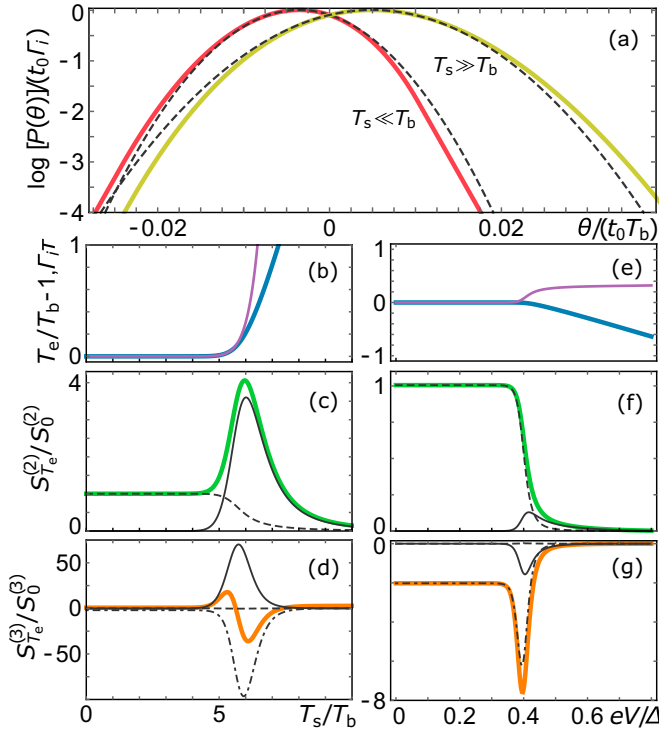
FIG. 3. (a) Temperature probability distribution $P(\theta)$ for $T_s = 10T_b$ (red, solid) and $T_s = 0.1T_b$ (yellow, solid), corresponding to injector cases (I) and (II), respectively. Dashed lines show the respective best Gaussian fits. In both plots $V = 0$, $T_b = 0.01\Delta/k_b$, $C = 20\Delta/T_b$, and $\tau\Gamma_i = 0.1$. (b)–(g) The first three cumulants as a function of T_s/T_b, at $V = 0$ [(b)–(d)] and eV/Δ, at $T_s = T_b$ [(e)–(g)]. In all panels $T_b = 0.01\Delta/k_b$, $C = 20\Delta/T_b$, and $\tau\Gamma_i = 0.1$ at $T_s = 5T_b$ and $eV = 0.4\Delta$, respectively. The total cumulants are shown with thick, solid lines. In (b) and (e), $\tau\Gamma_i$ is also shown (purple, thin solid). In (c), (d), (f), (g) the injector-absorber (thin, solid) and bath-absorber (thin, dashed) contributions to the respective cumulants are shown. In (d) and (g) the back-action component (dash dotted) is shown.

by (see appendix)

$$S_{T_e}^{(2)} = \frac{1}{\kappa^2}\langle\!\langle \mathcal{E}^2(T_e)\rangle\!\rangle,$$

$$S_{T_e}^{(3)} = \frac{1}{\kappa^3}\left[\langle\!\langle \mathcal{E}^3(T_e)\rangle\!\rangle + 3\langle\!\langle \mathcal{E}^2(T_e)\rangle\!\rangle\frac{d}{dT_e}\frac{\langle\!\langle \mathcal{E}^2(T_e)\rangle\!\rangle}{\kappa(T_e)}\right]. \quad (8)$$

In Eq. (8), we have $\kappa(T_e) = i\partial_{T_e}\partial_\xi F(\xi, T_e)|_{\xi=0}$, and all quantities are evaluated at $\overline{T}_e$. We note that the back action, besides modifying $\overline{T}_e$, is manifested as additional terms for the third [last term in Eq. (8)] and higher-order cumulants. These terms describe the effect of fluctuations of lower cumulants on higher ones [44], i.e., "noise of noise." In Figs. 3(b)–3(g), $\overline{T}_e$, $S_{T_e}^{(2)}$, and $S_{T_e}^{(3)}$ are plotted as functions of thermal ($V = 0$) and voltage ($T_s = T_b$) bias, respectively, for experimentally relevant parameters (see caption).

A. Thermal bias

We focus on the experimentally relevant regime $\beta \gg \ln(r) \gg 1$, with $\beta = \Delta/(k_B T_b)$ and $r = g\Delta/[T_b\kappa]$. Upon increasing T_s, the average temperature $\overline{T}_e = T_b[1 + 5rh(T_s)]^{1/5}$

shows [Fig. 3(b)] a crossover at $T_s \sim T_s^* \equiv \Delta/[k_B\ln(r)]$ from constant (dominated by bath coupling) to exponentially increasing $\sim e^{-\Delta/[5k_B T_s]}$ (dominated by injector coupling).

The temperature fluctuations $S_{T_e}^{(2)}$, normalized to the equilibrium phonon noise $S_0^{(2)} = 2k_B T_b^2/\kappa$, can be written as a sum of the bath and injector noise,

$$S_{T_e}^{(2)}/S_0^{(2)} = \frac{1 + q^6}{2q^8} + \frac{\beta(q^5 - 1)}{10q^8}, \quad (9)$$

where $q \equiv \overline{T}_e/T_b$. As shown in Fig. 3(c), upon increasing T_s the bath noise decreases while the injector noise first increases. The total noise peaks at $T_s \approx T_s^*$ and then decays towards zero, due to increasing thermal conductivity $\kappa(\overline{T}_e) = \kappa q^4$. The peak value, to leading order in $1/\beta \ll 1$, is $S_{T_e}^{(2)}/S_0^{(2)} \approx 0.035\beta$.

The third cumulant is plotted in Fig. 3(d). At low temperatures $T_s \ll T_s^*$, $S_{T_e}^{(3)}$ is dominated by the last term in Eq. (8), giving $S_{T_e}^{(3)}/S_0^{(3)} = -2$, with $S_0^{(3)} = 6k_B^2 T_b^3/\kappa^2$. Increasing T_s the cumulant changes sign twice around T_s^*, a consequence of a competition between the positive injector term and the negative back-action term. The analysis of the cumulants shows that T_s^* sets the upper limit for operation of the calorimeter; for $T_s \ll T_s^*$ we have well separated injection events, $\Gamma_i\tau \ll 1$, and the effect of the back action on the absorber temperature is negligible.

B. Voltage bias

The average temperature $\overline{T}_e$ as a function of V shows [Fig. 3(e)] a cooling effect [39], with a crossover around $V \sim V^* \equiv [\Delta - \ln(r)k_B T_b]/e$ from constant to close-to-linear decrease $k_B\overline{T}_e \approx (\Delta - eV)/\ln(r)$. The normalized fluctuations can be written as a sum of the bath ($\propto 1 + q^6$) and injector ($\propto 1 - q^5$) noise as, introducing $\tilde{\beta} = \beta(1 - eV/\Delta)$,

$$\frac{S_{T_e}^{(2)}}{S_0^{(2)}} = \frac{q^4}{2}\frac{1 + q^6 + (\tilde{\beta}/5)(1 - q^5)}{(q^6 + (\tilde{\beta}/5)(1 - q^5))^2}. \quad (10)$$

At $V < V^*$, the noise is dominated by the (equilibrium) phonon part [see Fig. 3(f)] while for $V > V^*$ the noise decreases monotonically with increasing V, due to increasing thermal conductivity $\kappa(\overline{T}_e) = \kappa(q^4 + \tilde{\beta}(1 - q^5)/[5q^2])$. The third cumulant $S_{T_e}^{(3)}$ is dominated, for $V < V^*$, by the back-action term, giving $S_{T_e}^{(3)}/S_0^{(3)} = -2$. With increasing bias the cumulant first becomes increasingly negative, reaching a minimum around V^* and thereafter decrease in absolute magnitude, towards zero, see Fig. 3(g). Most importantly, V^* sets the upper limit for V for a faithful calorimetric operation. Experimentally, a finite V can lead to simultaneous changes of $T_e(t)$ and T_s, not discussed here.

IV. OPERATION AND PERFORMANCE

Finally we discuss the experimental feasibility. While a standard dilution refrigerator reaches a temperature ~ 10 mK, careful design of the experiment is needed to reach that low $\overline{T}_e$. However, an equilibrium absorber electron temperature ~ 30 mK, setting the effective bath temperature T_b, is fully feasible. Moreover, C of a small metallic absorber at

$T_b \sim 30\,\text{mK}$ can be as low as $10^3 k_B$ [10], although some studies [35] indicate that thin films exhibit higher values. The values $C \sim 10^3 k_B$ and $T_b = 30\,\text{mK}$ yield a signal-to-noise ratio of order unity for an energy $\varepsilon \sim 100\,\mu\text{eV}$, see Fig. 1 for representative time traces. Possible ways to increase S/N are to employ a larger gap superconductor as injector and a lower C by using, e.g., a semiconducting or graphene [45] absorber.

V. CONCLUSIONS AND OUTLOOK

We have proposed and theoretically analyzed nanoscale quantum calorimetry of tunneling electrons in a hybrid superconducting setup. As our main result, we show that sub-meV calorimetry is feasible under optimized experimental conditions. Key for our analysis is a microscopic approach, treating all heat transfer events on an equal footing and fully accounting for back-action effects. Analyzing the resulting calorimeter temperature fluctuations allows us to derive conditions for a faithful calorimeter operation. Our results will spur advanced investigations of experimentally relevant phenomena, e.g., the effect of a nonequilibrium electron distribution of the absorber and the invasive effect of the temperature measurement.

APPENDIX: DETAILED CALCULATIONS

1. Monte Carlo simulations

Here we present some examples of Monte Carlo generated time traces of the temperature fluctuations. The simulations are fully taking into account both the stochastic injector events, transferring energy according to the CGF in Eq. (4) of the main text, and the stochastic phonon emission and absorption events. From the simulations we obtain numerical values of the average temperature, noise, and skewness. Key expressions like Eqs. (8), (9), and (10) of the main text have been found to be in perfect agreement with the Monte Carlo simulations.

In Fig. 4, we show examples of time traces for $T_b = 5\,\text{mK}$, $T_b = 30\,\text{mK}$, and $T_b = 100\,\text{mK}$, respectively, to illustrate the effect of phonon noise at different temperatures. In all cases, $\varepsilon = 200\,\mu\text{eV}$, $C = 1000 k_B$, and time is chosen such that an injector event takes place at $t = 0$. The three cases correspond to $\Delta T_e / \sqrt{\langle \delta T_e^2 \rangle} = 15, 2.4$ and 0.73, respectively. As clearly seen, at low temperatures [see Fig. 4(a)], the background noise is almost negligible compared to the temperature spike induced by the injector. For more experimentally realistic settings with intermediate temperatures [see Fig. 4(b)], the temperature spike of the injector is still clearly visible, although the background noise is no longer negligible. At even higher temperatures [see Fig. 4(c)], the temperature spike induced by the injector drowns in phonon noise and it gets difficult to identify the injector events.

2. Generating function for the injector-absorber energy transfer

Here we derive the cumulant generating function for the superconducting injector given in Eq. (5) of the main text. Our starting point is Eq. (4) of the main text,

$$F_i(\xi_i, T_e) = \int d\varepsilon [\Gamma_+^i (e^{i\xi_i \varepsilon} - 1) + \Gamma_-^i (e^{-i\xi_i \varepsilon} - 1)], \quad \text{(A1)}$$

with rates $\Gamma_\pm^i(\varepsilon) = (G_T/e^2)\nu_S(\varepsilon - eV)f_\pm(\varepsilon - eV, T_s)f_\mp(\varepsilon, T_e)$, where $\nu_S(\varepsilon) = |\varepsilon|/\sqrt{\varepsilon^2 - \Delta^2}\,\theta(|\varepsilon| - \Delta)$ is the normalized superconducting density of state, $f_+(\varepsilon, T) = (e^{\varepsilon/[k_B T]} + 1)^{-1}$ and $f_-(\varepsilon, T) = 1 - f_+(\varepsilon, T)$.

For $k_B T \ll \Delta - e|V|$, $T = T_s, T_e$, only the tails of the Fermi functions contribute to the integral. Equation (A1) can then be written as

$$
\begin{aligned}
F_i(\xi_i, T_e) = \frac{G_T}{e^2} &\left(\int_{\Delta + eV}^{\infty} d\varepsilon \frac{\varepsilon - eV}{\sqrt{(\varepsilon - eV)^2 - \Delta^2}} [e^{-(\varepsilon - eV)/[k_B T_s]}(e^{i\xi_i \varepsilon} - 1) + e^{-\varepsilon/[k_B T_e]}(e^{-i\xi_i \varepsilon} - 1)] \right. \\
&- \left. \int_{-\infty}^{-\Delta + eV} d\varepsilon \frac{\varepsilon - eV}{\sqrt{(\varepsilon - eV)^2 - \Delta^2}} [e^{\varepsilon/[k_B T_e]}(e^{i\xi_i \varepsilon} - 1) + e^{(\varepsilon - eV)/[k_B T_s]}(e^{-i\xi_i \varepsilon} - 1)] \right) \\
= \frac{G_T}{e^2} &\left(\int_{\Delta + eV}^{\infty} d\varepsilon \frac{\varepsilon - eV}{\sqrt{(\varepsilon - eV)^2 - \Delta^2}} [e^{-(\varepsilon - eV)/[k_B T_s]}(e^{i\xi_i \varepsilon} - 1) + e^{-\varepsilon/[k_B T_e]}(e^{-i\xi_i \varepsilon} - 1)] \right. \\
&+ \left. \int_{\Delta - eV}^{\infty} d\varepsilon \frac{\varepsilon + eV}{\sqrt{(\varepsilon + eV)^2 - \Delta^2}} [e^{-(\varepsilon + eV)/[k_B T_s]}(e^{i\xi_i \varepsilon} - 1) + e^{-\varepsilon/[k_B T_e]}(e^{-i\xi_i \varepsilon} - 1)] \right). \quad \text{(A2)}
\end{aligned}
$$

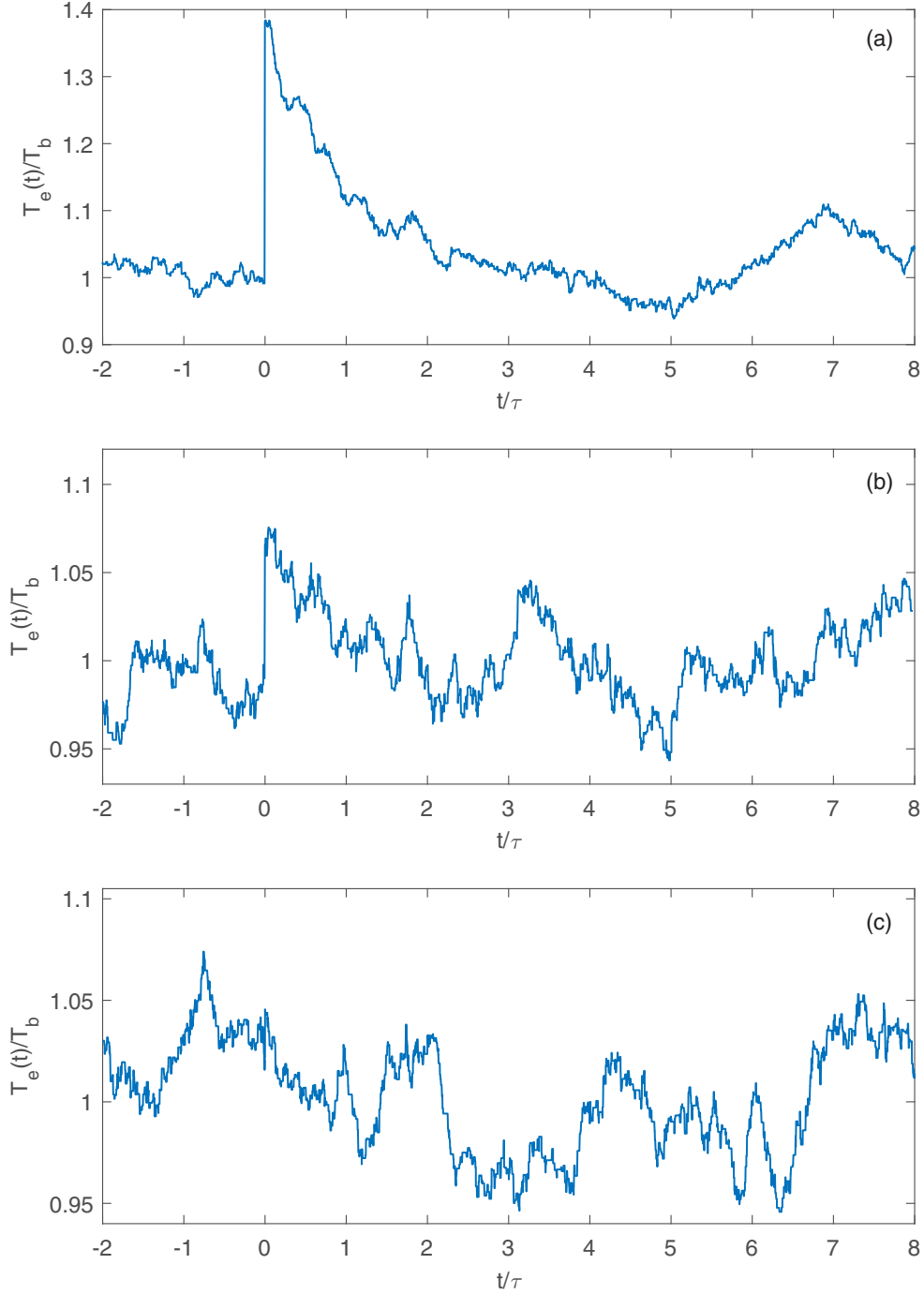FIG. 4. Examples of Monte Carlo generated time traces of the temperature fluctuations for (a) $T_b = 5\,\text{mK}$, (b) $T_b = 30\,\text{mK}$, and (c) $T_b = 100\,\text{mK}$. Every time trace contains an injector event at $t = 0$. In all cases, $C = 1000 k_B$, $\varepsilon = 200\,\mu\text{eV}$, and τ denotes the relaxation time.

Now, evaluating the integrals explicitly, we obtain

$$F_i(\xi_i, T_e) = \sqrt{\frac{2}{\pi}} g \left(K_1 \left[\frac{\Delta}{k_B T_s} - i \xi_i \Delta \right] \cos \left[e V \xi_i \right] + K_1 \left[\frac{\Delta}{k_B T_e} + i \xi_i \Delta \right] \cosh \left[\frac{e V}{k_B T_e} + i e V \xi_i \right] \right.$$

$$\left. - K_1 \left[\frac{\Delta}{k_B T_s} \right] - K_1 \left[\frac{\Delta}{k_B T_e} \right] \cosh \left[\frac{e V}{k_B T_e} \right] \right), \tag{A3}$$

where $g = \frac{\sqrt{2\pi}G_T\Delta}{e^2}$ and $K_n[x]$ denotes the nth modified Bessel function of the second kind. Using that $k_BT \ll \Delta$, $T = T_s, T_e$, we simplify the Bessel functions as

$$K_1\left[\frac{\Delta}{k_BT} \pm i\xi_i\Delta\right] \approx \sqrt{\frac{\pi}{2}}h(T)e^{\mp i\xi_i\Delta}, \tag{A4}$$

with $h(T) = \sqrt{\frac{k_BT}{\Delta}}e^{-\frac{\Delta}{k_BT}}$. This yields the following expression for the generating function for the injector-absorber junction:

$$F_i(\xi_i, T_e) = g\left(h(T_s)e^{i\xi_i\Delta}\cos[eV\xi_i] + h(T_e)e^{-i\xi_i\Delta}\cosh\left[\frac{eV}{k_BT_e} + ieV\xi_i\right] - h(T_s) - h(T_e)\cosh\left[\frac{eV}{k_BT_e}\right]\right). \tag{A5}$$

a. No applied bias (case I and II)

For $V = 0$, Eq. (A5) simplifies to

$$F_i(\xi_i, T_e) = g[h(T_s)(e^{i\xi_i\Delta} - 1) + h(T_e)(e^{-i\xi_i\Delta} - 1)]. \tag{A6}$$

For $T_s \ll T_e$ ($T_s \gg T_e$), the second (first) term is negligible, yielding case (I) [(II)] in Eq. (5) of the main text. In both cases, the statistics correspond to Poissonian processes with an energy of Δ transferred in each elementary process.

b. Finite bias (case III)

For $eV \gg kT_e$, we obtain from Eq. (A5)

$$F_i(\xi_i, T_e) = g\left(\frac{h(T_s)}{2}[e^{i(\Delta+eV)\xi_i} - 1 + e^{i(\Delta-eV)\xi_i} - 1]\right.$$
$$\left. + \frac{h(T_e)}{2}[e^{-i(\Delta-eV)\xi_i} - 1]\right). \tag{A7}$$

If $T_s(1 - eV/\Delta) \ll T_e$, the first part is negligible and the cumulant generating function reduces to

$$F_i(\xi_i, T_e) = gh(T_e)e^{\frac{eV}{k_BT_e}}(e^{i(eV-\Delta)\xi_i} - 1), \tag{A8}$$

which corresponds to case (III) in Eq. (5) of the main text.

3. Generating function for the bath-absorber energy transfer

At low temperatures, with a weak electron-phonon coupling, Fermi's golden rule yields the following counting field resolved rates

$$\tilde{\Gamma}^b_\pm(\xi) = \frac{2\pi}{\hbar}\int dE_\mathbf{k}N_e(E_\mathbf{k})f(E_\mathbf{k})\int d\mathbf{q}N_b(\mathbf{q})n_\pm(\varepsilon_\mathbf{q})\mathcal{M}^2$$
$$\times\left[1 - f(E_{\mathbf{k}\pm\mathbf{q}})\right]\delta(E_\mathbf{k} - E_{\mathbf{k}\pm\mathbf{q}} + \varepsilon_\mathbf{q})e^{\pm i\varepsilon_q\xi}, \tag{A9}$$

where $\tilde{\Gamma}_+(\xi)$ [$\tilde{\Gamma}_-(\xi)$] denotes the counting field resolved absorption (emission) rate of phonons, $E_\mathbf{k}$ ($\varepsilon_\mathbf{q}$) is the energy of an electron (phonon) with momentum $\mathbf{k}$ ($\mathbf{q}$), $N_e(\varepsilon)$ ($N_b(\varepsilon)$) is the density of states of electrons (phonons) on the island, $f(\varepsilon) = (\exp[\varepsilon/kT_e] + 1)^{-1}$ is the Fermi function for the electrons, $n_+(\varepsilon) = (\exp[\varepsilon/(kT_b)] - 1)^{-1}$ is the Bose distribution for the phonons, with $n_-(\varepsilon) = 1 + n_+(\varepsilon)$, and $\mathcal{M}$ is the coupling strength matrix element for electron-phonon scattering. The signs of the counting fields have been chosen such that positive energy corresponds to an inflow of energy to the electrons from the phonons.

At low temperatures, all relevant scattering processes occur around the Fermi level, i.e., $|\mathbf{k}| \approx |\mathbf{k}_F|$, $|\mathbf{q}| \ll |\mathbf{k}_F|$, and $N(E_\mathbf{k}) \approx N_e$. We use a parabolic dispersion relation for the electrons in the metal, $E_\mathbf{k} = \frac{\hbar^2k^2}{2m} \equiv E_k$. Furthermore, the

phonons are treated as longitudinal ones within the Debye model, i.e., $N_b(\mathbf{q}) = \mathcal{V}/(2\pi)^3 \equiv N_b$ and $\varepsilon_\mathbf{q} = \hbar c_lq \equiv \varepsilon_q$, where c_l is the velocity of the phonons. For a scalar deformation potential, $\mathcal{M}^2 = \mathcal{M}_0^2q$ and Eq. (A9) can be written as

$$\tilde{\Gamma}^b_\pm(\xi) = \frac{2\pi\mathcal{M}_0^2N_eN_b}{\hbar}\int dE_\mathbf{k}f(E_k)\int d\mathbf{q}qn_\pm(\varepsilon_q)e^{\pm i\varepsilon_q\xi}$$
$$\times[1 - f(E_{\mathbf{k}\pm\mathbf{q}})\delta(E_k - E_{\mathbf{k}\pm\mathbf{q}} \pm \varepsilon_q)]. \tag{A10}$$

Evaluating the integral over $\mathbf{q}$, we obtain

$$\tilde{\Gamma}^b_\pm(\xi) = \frac{2\pi\mathcal{M}_0^2N_eN_b}{\hbar^3c_l^2}\int dE_\mathbf{k}f(E_k)\int d\varepsilon\varepsilon^2\frac{2\pi m}{\hbar^3k_Fc_l}$$
$$\times[1 - f(E_k \pm \varepsilon)]n_\pm(\varepsilon)e^{\pm i\varepsilon\xi}. \tag{A11}$$

Now, we rewrite the integral as

$$\tilde{\Gamma}^b_\pm(\xi) = \frac{(2\pi)^2m\mathcal{M}_0^2N_eN_b}{\hbar^6c_l^3k_F}\int d\varepsilon\varepsilon^2n_\pm(\varepsilon)e^{\pm i\varepsilon\xi}$$
$$\times\int dEf(E)[1 - f(E \pm \varepsilon)], \tag{A12}$$

or

$$\tilde{\Gamma}^b_\pm(\xi) = \frac{\mathcal{V}\mathcal{M}_0^2N_e}{2\pi\hbar^5c_l^3v_F}\int d\varepsilon\varepsilon^2n_\pm(\varepsilon)e^{\pm i\varepsilon\xi}$$
$$\times\int dEf(E)[1 - f(E \pm \varepsilon)], \tag{A13}$$

where v_F is the Fermi velocity of the electrons. The prefactor corresponds to $\Sigma\mathcal{V}/[24k_B^5\zeta(5)]$, while the integral over E gives

$$\int_{-\infty}^{\infty}dEf(E)[1 - f(E \pm \varepsilon)] = \varepsilon n_\mp(\varepsilon, T_e), \tag{A14}$$

where we have introduced a Bose distribution with explicit temperature dependence. We then obtain

$$\tilde{\Gamma}^b_\pm(\xi) = \frac{\Sigma\mathcal{V}}{24k_B^5\zeta(5)}\int d\varepsilon\varepsilon^3n_\pm(\varepsilon, T_b)n_\mp(\varepsilon, T_e)e^{\pm i\varepsilon\xi}. \tag{A15}$$

The cumulant generating function is given by $F_b(\xi_b, T_b) = \Gamma^b_+(\xi_b) + \Gamma^b_-(\xi_b) - \Gamma^b_+(0) - \Gamma^b_-(0)$, or, equivalently,

$$F_b(\xi_b, T_b) = \int_0^{\infty}d\varepsilon[\Gamma^b_+(\varepsilon)(e^{i\xi_b\varepsilon} - 1) + \Gamma^b_-(\varepsilon)(e^{-i\xi_b\varepsilon} - 1)], \tag{A16}$$

with $\Gamma_{\pm}^{b}(\varepsilon) = \frac{\Sigma\mathcal{V}}{24k_{B}^{5}\zeta(5)}\varepsilon^{3}n_{\pm}(\varepsilon, T_{b})n_{\mp}(\varepsilon, T_{e})$. The cumulants are given by $S_{b}^{(n)} = \frac{\partial F_{b}(\xi_{b}, T_{b})}{\partial\xi_{b}}|_{\xi_{b}=0}$, yielding

$$S_{b}^{(n)} = \frac{\Sigma\mathcal{V}}{24k_{B}^{5}\zeta(5)}\int_{0}^{\infty}d\varepsilon\varepsilon^{3+n}[n_{+}(\varepsilon, T_{b})n_{-}(\varepsilon, T_{e})$$
$$\pm n_{-}(\varepsilon, T_{b})n_{+}(\varepsilon, T_{e})], \quad (A17)$$

with $+$ for n even and $-$ for n odd. For odd n, we obtain

$$S_{b}^{(n)} = \frac{\Sigma\mathcal{V}}{48k_{B}^{5}\zeta(5)}\int_{0}^{\infty}d\varepsilon\varepsilon^{3+n}$$
$$\times\left[\coth\left(\frac{\varepsilon}{2k_{B}T_{b}}\right) - \coth\left(\frac{\varepsilon}{2k_{B}T_{e}}\right)\right]$$
$$= \Sigma\mathcal{V}k_{B}^{n-1}\frac{\zeta(n+3)(n+3)!}{24\zeta(5)}(T_{b}^{n+4} - T_{e}^{n+4}), \quad (A18)$$

while for even n, we obtain

$$S_{b}^{(n)} = \frac{\Sigma\mathcal{V}}{48k_{B}^{5}\zeta(5)}\int_{0}^{\infty}d\varepsilon\varepsilon^{3+n}$$
$$\times\left[\coth\left(\frac{\varepsilon}{2k_{B}T_{b}}\right)\coth\left(\frac{\varepsilon}{2k_{B}T_{e}}\right) - 1\right]$$
$$\approx \Sigma\mathcal{V}k_{B}^{n-1}\frac{\zeta(n+4)(n+3)!}{24\zeta(5)}(T_{b}^{n+4} + T_{e}^{n+4}). \quad (A19)$$

In the last step, we have made use of the following approximation:

$$I_{1} \equiv \int_{0}^{\infty}d\varepsilon \, \varepsilon^{3+n}[\coth(\varepsilon r)\coth(\varepsilon) - 1]$$
$$\approx \int_{0}^{\infty}d\varepsilon \frac{\varepsilon^{3+n}}{2}[\coth^{2}(\varepsilon) - 1]\left(1 + \frac{1}{r^{6}}\right) \equiv I_{2}. \quad (A20)$$

To estimate the accuracy of this approximation, we first perform a change of variables $\varepsilon \to \varepsilon r$ in the second term in I_{2} to obtain

$$I_{2} = \int_{0}^{\infty}d\varepsilon \, \varepsilon^{3+n}\left[\frac{\coth^{2}(\varepsilon) + \coth^{2}(\varepsilon r)}{2} - 1\right] \quad (A21)$$

with which we get

$$I_{2} - I_{1} = \int_{0}^{\infty}d\varepsilon \frac{\varepsilon^{3+n}}{2}[\coth(\varepsilon) - \coth(\varepsilon r)]^{2}. \quad (A22)$$

By noting that $\coth(\varepsilon) \geqslant \coth(\varepsilon r) \geqslant 1$ for any $\varepsilon \geqslant 0$ and $r \geqslant 1$, we have that

$$\frac{I_{2} - I_{1}}{I_{2}} \leqslant \frac{\int_{0}^{\infty}d\varepsilon \, \varepsilon^{3+n}[\coth(\varepsilon) - 1]^{2}}{\int_{0}^{\infty}d\varepsilon \, \varepsilon^{3+n}[\coth^{2}(\varepsilon) - 1]}$$
$$\leqslant \frac{\int_{0}^{\infty}d\varepsilon \, \varepsilon^{5}[\coth(\varepsilon) - 1]^{2}}{\int_{0}^{\infty}d\varepsilon \, \varepsilon^{5}[\coth^{2}(\varepsilon) - 1]} = 1 - \frac{\pi^{6}}{945\zeta(5)}$$
$$\approx 0.0189 \quad (A23)$$

with the first inequality becoming an equality only for $r \to \infty$.

4. Stochastic path integral formulation

The starting point for the derivation of the full statistics of the time-integrated temperature fluctuations

$\theta = \int_{0}^{t_{0}}dt[T_{e}(t) - \overline{T}_{e}]$ is the generating functions for energy transfers between the injector and the absorber, $\Delta t F_{i}[\xi_{i}(t), T_{e}(t)]$, and the bath and the absorber, $\Delta t F_{b}[\xi_{b}(t), T_{e}(t)]$, during a time interval $[t, t + \Delta t]$. The length of the time interval Δt is so short that the absorber temperature is only marginally changed, $T_{e}(t + \Delta t) \approx T_{e}(t) + \Delta T_{e}(t)$, where $\Delta T_{e}(t) \ll T_{e}(t)$. This requires Δt to be much shorter than the time scale over which $T_{e}(t)$ changes appreciably, typically set by τ.

In an interval Δt, for transferred energies ΔE_{i} and ΔE_{b}, the corresponding energy currents are $I_{Ei} = \Delta E_{i}/\Delta t$ and $I_{Eb} = \Delta E_{b}/\Delta t$, for the injector-absorber and bath-absorber transfers, respectively. For the entire measurement time t_{0}, taking the continuum-in-time limit, we can write the joint, unconditioned probability distribution of energy currents as a product of the individual probabilities as

$$P[I_{Ei}, I_{Eb}] = P[I_{Ei}]P[I_{Eb}], \quad (A24)$$

where the probabilities $P[I_{Ei}]$, $P[I_{Eb}]$ conveniently can be written as stochastic path integrals as

$$P[I_{Ei}] = \int \mathcal{D}[\xi_{i}]e^{\int_{0}^{t_{0}}dt(-iI_{Ei}(t)\xi_{i}(t) + F_{i}[\xi_{i}(t), T_{e}(t)])}, \quad (A25)$$

and

$$P[I_{Eb}] = \int \mathcal{D}[\xi_{b}]e^{\int_{0}^{t_{0}}dt(-iI_{Eb}(t)\xi_{b}(t) + F_{b}[\xi_{b}(t), T_{e}(t)])}. \quad (A26)$$

To account for the effect of the transferred energy, with resulting fluctuations of $T_{e}(t)$, and following back action on the statistics on the transfer events themselves, we have the absorber energy $E(t)$ conservation equation

$$\frac{dE(t)}{dt} = I_{Ei}(t) + I_{Eb}(t). \quad (A27)$$

Importantly, the total energy of the absorber is directly related to the temperature via the relation $E(t) = C[T_{e}(t)]T_{e}(t)/(2C)$ with $C[T_{e}(t)] \propto T_{e}(t)$. The conditioned probability for the realizations of the energy currents is then given by the unconstrained one multiplied by a functional δ function as

$$P[I_{Ei}, I_{Eb}]\delta\left[\frac{dE(t)}{dt} - I_{Ei}(t) + I_{Ei}(t)\right]. \quad (A28)$$

Integrating the constrained probability over the energy currents we get, writing the δ function as a functional Fourier transform and inserting the expression in Eq. (A24),

$$\int \mathcal{D}[I_{Ei}]\mathcal{D}[\xi_{i}]\mathcal{D}[I_{Eb}]\mathcal{D}[\xi_{b}]\mathcal{D}[\xi] \exp\left[\int_{0}^{t_{0}}dt H(t)\right], \quad (A29)$$

where $H(t) = H[t, I_{Ei}(t)\xi_{i}(t), I_{Eb}(t)\xi_{b}(t), \xi(t)]$ is

$$H(t) = i\xi(t)\left(\frac{dE(t)}{dt} - I_{Ei}(t) - I_{Eb}(t)\right) - iI_{Ei}(t)\xi_{i}(t)$$
$$+ F_{i}[\xi_{i}(t), T_{e}(t)] - iI_{Eb}(t)\xi_{b}(t)$$
$$+ F_{b}[\xi_{b}(t), T_{e}(t)]. \quad (A30)$$

We can now perform the integrals over $I_{Ei}(t)$ and $I_{Eb}(t)$, giving functional delta functions $\delta[\xi_{i}(t) - \xi(t)]$ and $\delta[\xi_{b}(t) - \xi(t)]$ and hence the total, constrained probability

$$\int \mathcal{D}[\xi] \exp[\int_{0}^{t_{0}} G[t, \xi(t), T_{e}(t)]], \quad (A31)$$

where

$$G[t, \xi(t), T_e(t)] = i\xi(t)\frac{dE(t)}{dt} + F_i[\xi(t), T_e(t)] + F_b[\xi(t), T_e(t)]. \quad (A32)$$

This expression thus gives the probability distribution of realizations of the total energy change, $dE(t)/dt$. To access the statistics of the realizations of the temperature we conveniently multiply the obtained probability distribution by a delta function $\delta[T(t) - T_e(t)]$, recalling the relation between $E(t)$ and $T_e(t)$, and integrate over $E(t)$ giving

$$P[T] = \int \mathcal{D}[\chi] e^{\int_0^{t_0} dt(-i\chi(t)T(t) + \lambda[t, \chi(t)])}, \quad (A33)$$

where

$$e^{\int_0^{t_0} dt\lambda[t,\chi(t)]} = \int \mathcal{D}[\xi]\mathcal{D}[E] e^{\int_0^{t_0} dt(i\chi(t)T_e(t) + G[t,\xi(t),T_e(t)])} \quad (A34)$$

is a stochastic path integral over $\xi(t)$, $E(t)$.

Long time limit

In the limit of a long measurement time t_0 we can neglect the time dependence of the variables and write the probability distribution of the time-integrated temperature $\theta = \int_0^{t_0} [T_e(t) - \overline{T}_e] dt$ as (up to phase factor shifting the distribution)

$$P(\theta) = \frac{1}{2\pi} \int d\chi \exp[-i\chi\theta + \lambda(\chi)], \quad (A35)$$

where

$$e^{\lambda(\chi)} = \int d\xi dE \exp[t_0 S(\chi, \xi, T_e)] \quad (A36)$$

and

$$S(\chi, \xi, T_e) = i\chi(T_e - \overline{T}_e) + F_i[\xi, T_e] + F_b[\xi, T_e]. \quad (A37)$$

Solving this equation in the saddle point approximation we get the generating function, to exponential accuracy, as

$$\lambda(\chi) = t_0 S(\chi, \xi^*, T_e^*), \quad (A38)$$

where $\xi^* = \xi^*(\chi)$ and $T_e^* = T_e^*(\chi)$ are the solutions of the saddle point equations

$$\frac{\partial S}{\partial \xi} = \frac{\partial F_i}{\partial \xi} + \frac{\partial F_b}{\partial \xi} = 0$$

$$\frac{\partial S}{\partial E} \propto \frac{\partial S}{\partial T_e} = i\chi + \frac{\partial F_i}{\partial T_e} + \frac{\partial F_b}{\partial T_e} = 0. \quad (A39)$$

From Eq. (A39) and $\lambda(\chi)$ we obtain the low-frequency cumulants of the temperature fluctuations as $S_{T_e}^{(n)} = (1/t_0)(-i)^n \partial_\chi^n \lambda(\chi)|_{\chi=0}$. In terms of $\langle\langle \mathcal{E}^n(T_e) \rangle\rangle = (-i)^n \partial_\xi^n F(\xi, T_e)|_{\xi=0}$, the cumulants of the absorber energy currents, the average temperature $\overline{T}_e$ is found from $\langle \mathcal{E}(\overline{T}_e) \rangle = 0$, yielding the equation

$$h(T_s) + h(\overline{T}_e)\left[-\cosh\left(\frac{eV}{k_B \overline{T}_e}\right) + \frac{eV}{\Delta} \sinh\left(\frac{eV}{k_B \overline{T}_e}\right) \right]$$

$$= \frac{1}{5r}\left(\frac{\overline{T}_e^5}{T_b^5} - 1\right), \quad (A40)$$

where $h(T) = \sqrt{\frac{k_B T}{\Delta}} e^{-\frac{\Delta}{k_B T}}$ as before and $r = \frac{\sqrt{2\pi} G_T \Delta^2}{T_b e^2 \kappa}$. The second and third temperature cumulants, experimentally most relevant, are given by

$$S_{T_e}^{(2)} = \frac{1}{\kappa^2} \langle\langle \mathcal{E}^2(T_e) \rangle\rangle,$$

$$S_{T_e}^{(3)} = \frac{1}{\kappa^3}\left[\langle\langle \mathcal{E}^3(T_e) \rangle\rangle + 3\langle\langle \mathcal{E}^2(T_e) \rangle\rangle \frac{d}{dT_e} \frac{\langle\langle \mathcal{E}^2(T_e) \rangle\rangle}{\kappa(T_e)} \right], \quad (A41)$$

where $\kappa(T_e) = i\partial_{T_e}\partial_\xi F(\xi, T_e)|_{\xi=0}$, the heat conductance, and all quantities in Eq. (A41) are evaluated at $\overline{T}_e$. This is Eq. (8) of the main text.

Of particular interest is the regime $\tau \ll 1/\Gamma_i$, with well separated energy injection events. Then $\overline{T}_e \approx T_b + \Delta T$, with $\Delta T = \Gamma_i \langle \varepsilon \rangle / \kappa$ and $\kappa \equiv \kappa(T_b)$, deviates negligibly from T_b. The temperature noise $S_{T_e}^{(2)}$ in Eq. (A41) becomes, to leading order in $\Delta T / T_b \ll 1$,

$$\frac{S_{T_e}^{(2)}}{S_0^{(2)}} = \frac{1}{2z^2}\left[1 + \left(\frac{\overline{T}_e}{T_b}\right)^6 \right] + \frac{r\beta}{2z^2}\left[h(T_s)\left[1 + \left(\frac{eV}{\Delta}\right)^2 \right] \right.$$

$$\left. + h(\overline{T}_e) H(\overline{T}_e, V) \right], \quad (A42)$$

where $S_0^{(2)} = \frac{2k_B T_b^2}{\kappa}$, $\beta = \frac{\Delta}{k_B T_b}$, $H(T, V) = [1 + (\frac{eV}{\Delta})^2]\cosh(\frac{eV}{k_B T}) - 2\frac{eV}{\Delta}\sinh(\frac{eV}{k_B T})$ and

$$z \equiv \frac{\kappa(T_e)}{\kappa} = \left(\frac{\overline{T}_e}{T_b}\right)^4 + r\beta\left(\frac{T_b}{\overline{T}_e}\right)^2 h(\overline{T}_e) H(\overline{T}_e, V). \quad (A43)$$

For only thermal bias, we obtain from Eq. (A40)

$$\Delta T = rT_b\left(h(T_s) + h(T_b) \right.$$

$$\left. \times \left[-\cosh\left(\frac{eV}{k_B T_b}\right) + \frac{eV}{\Delta}\sinh\left(\frac{eV}{k_B T_b}\right) \right] \right). \quad (A44)$$

Furthermore, $H(\overline{T}_e, V) = 1$. If $\beta \gg \ln(r) \gg 1$, we have $z = q^4$, where $q = \frac{\overline{T}_e}{T_b}$. The normalized second cumulant in Eq. (A42) then reduces to

$$\frac{S_{T_e}^{(2)}}{S_0^{(2)}} = \frac{1 + q^6 + (\beta/5)[q^5 - 1]}{2\tau^8} \quad (A45)$$

which is Eq. (9) of the main text.

For voltage bias only, $T_s = T_b$, and $rh(T_b) \ll 1$, Eq. (A40) reduces to

$$e^{-(\Delta - eV)/[k_B \overline{T}_e]} = \frac{2}{5r} \frac{\Delta^{3/2}}{\sqrt{\overline{T}_e}(\Delta - eV)}\left(1 - \frac{\overline{T}_e^5}{T_b^5} \right). \quad (A46)$$

Furthermore, we have $z = q^4 + \frac{\tilde{\beta}_b(1 - q^5)}{5q^2}$, where $\tilde{\beta} = \beta(1 - \frac{eV}{\Delta})$. The normalized second cumulant in Eq. (A42) then reduces to

$$\frac{S_{T_e}^{(2)}}{S_0^{(2)}} = \frac{q^4}{2} \frac{1 + q^6 + (\beta/5)[1 - q^5]}{(q^6 + (\tilde{\beta}_b/5)(1 - q^5))^2}, \quad (A47)$$

which is Eq. (10) of the main text.

[1] C. Kilbourne Stahle, D. McCammon, and K. D. Irwin, Phys. Today **52**, 32 (1999).

[2] D. McCammon, W. Cui, M. Juda, J. Morgenthaler, J. Zhang, R. Kelley, S. Holt, G. Madejski, S. Moseley, and A. Szymkowiak, Nucl. Instrum. Methods Phys. Res., Sect. A **326**, 157 (1993).

[3] M. Nahum and J. M. Martinis, Appl. Phys. Lett. **66**, 3203 (1995).

[4] D. R. Schmidt, K. W. Lehnert, A. M. Clark, W. D. Duncan, K. D. Irwin, N. Miller, and J. N. Ullom, Appl. Phys. Lett. **86**, 053505 (2005).

[5] J. Overley, H. Lefevre, I. Nolt, J. Radostitz, S. Predko, and P. Ade, Nucl. Instrum. Methods Phys. Res., Sect. B **10-11**, 928 (1985).

[6] N. Coron, G. Dambier, G. J. Focker, P. G. Hansen, G. Jegoudez, B. Jonson, J. Leblanc, J. P. Moalic, H. L. Ravn, H. H. Stroke, and O. Testard, Nature (London) **314**, 75 (1985).

[7] C. Enss, *Cryogenic Particle Detection* (Springer Berlin Heidelberg, Berlin, Heidelberg, 2005).

[8] D. R. Schmidt, C. S. Yung, and A. N. Cleland, Appl. Phys. Lett. **83**, 1002 (2003).

[9] D. R. Schmidt, C. S. Yung, and A. N. Cleland, Phys. Rev. B **69**, 140301 (2004).

[10] S. Gasparinetti, K. L. Viisanen, O.-P. Saira, T. Faivre, M. Arzeo, M. Meschke, and J. P. Pekola, Phys. Rev. Applied **3**, 014007 (2015).

[11] J. Govenius, R. E. Lake, K. Y. Tan, and M. Möttönen, Phys. Rev. Lett. **117**, 030802 (2016).

[12] J. Wei, D. Olaya, B. S. Karasik, S. V. Pereverzev, A. V. Sergeev, and M. E. Gershenson, Nat. Nanotechnol. **3**, 496 (2008).

[13] B. S. Karasik, A. V. Sergeev, and D. E. Prober, IEEE Trans. Terahertz Sci. **1**, 97 (2011).

[14] J. P. Pekola, P. Solinas, A. Shnirman, and D. V. Averin, New J. Phys. **15**, 115006 (2013).

[15] S. Gasparinetti, P. Solinas, A. Braggio, and M. Sassetti, New J. Phys. **16**, 115001 (2014).

[16] M. Silaev, T. T. Heikkilä, and P. Virtanen, Phys. Rev. E **90**, 022103 (2014).

[17] J. P. Pekola, Nat. Phys. **11**, 118 (2015).

[18] A. Hofmann, V. F. Maisi, J. Basset, C. Reichl, W. Wegscheider, T. Ihn, K. Ensslin, and C. Jarzynski, Phys. Status Solidi B **254**, 1600546 (2017).

[19] C. Jarzynski, Phys. Rev. Lett. **78**, 2690 (1997).

[20] G. E. Crooks, Phys. Rev. E **60**, 2721 (1999).

[21] M. Campisi, P. Talkner, and P. Hänggi, Phys. Rev. Lett. **102**, 210401 (2009).

[22] P. Talkner and P. Hänggi, J. Phys. A: Math. Theor. **40**, F569 (2007).

[23] T. Albash, D. A. Lidar, M. Marvian, and P. Zanardi, Phys. Rev. E **88**, 032146 (2013).

[24] A. E. Rastegin and K. Życzkowski, Phys. Rev. E **89**, 012127 (2014).

[25] K. Schwab, E. A. Henriksen, J. M. Worlock, and M. L. Roukes, Nature (London) **404**, 974 (2000).

[26] L. del Rio, J. Åberg, R. Renner, O. Dahlsten, and V. Vedral, Nature (London) **474**, 61 (2011).

[27] J. M. R. Parrondo, J. M. Horowitz, and T. Sagawa, Nat. Phys. **11**, 131 (2015).

[28] T. L. van den Berg, F. Brange, and P. Samuelsson, New J. Phys. **17**, 075012 (2015).

[29] F. C. Wellstood, C. Urbina, and J. Clarke, Phys. Rev. B **49**, 5942 (1994).

[30] B. Karimi and J. P. Pekola, Phys. Rev. Appl. **10**, 054048 (2018).

[31] B. A. Muzykantskii and D. E. Khmelnitskii, Phys. Rev. B **50**, 3982 (1994).

[32] W. Belzig, *Quantum Noise in Mesoscopic Physics*, edited by Y. V. Nazarov (Kluwer, Dordrecht, 2003).

[33] M. Kindermann and S. Pilgram, Phys. Rev. B **69**, 155334 (2004).

[34] D. Golubev and L. Kuzmin, J. Appl. Phys. **89**, 6464 (2001).

[35] K. L. Viisanen and J. P. Pekola, Phys. Rev. B **97**, 115422 (2018).

[36] G. D. Mahan, *Many-Particle Physics* (Springer, US, 2000).

[37] J. Voutilainena, M. A. Laakso, and T. T. Heikkilä, J. Appl. Phys. **107**, 064508 (2010).

[38] J. P. Pekola and B. Karimi, J. Low Temp. Phys. **191**, 373 (2018).

[39] F. Giazotto, T. T. Heikkilä, A. Luukanen, A. M. Savin, and J. P. Pekola, Rev. Mod. Phys. **78**, 217 (2006).

[40] T. T. Heikkilä and Y. V. Nazarov, Phys. Rev. Lett. **102**, 130605 (2009).

[41] M. A. Laakso, T. T. Heikkilä, and Y. V. Nazarov, Phys. Rev. Lett. **104**, 196805 (2010).

[42] M. A. Laakso, T. T. Heikkilä, and Y. V. Nazarov, Phys. Rev. Lett. **108**, 067002 (2012).

[43] F. Battista, M. Moskalets, M. Albert, and P. Samuelsson, Phys. Rev. Lett. **110**, 126602 (2013).

[44] A. N. Jordan, E. Sukhorukov, and S. Pilgram, J. Math. Phys. **45**, 4386 (2004).

[45] E. D. Walsh, D. K. Efetov, G.-H. Lee, M. Heuck, J. Crossno, T. A. Ohki, P. Kim, D. Englund, and K. C. Fong, Phys. Rev. Applied **8**, 024022 (2017).